Molecular dynamics model for the antibactericity of textured surfaces

G. Lazzini[a], A.H.A. Lutey[a], L. Romoli[a], F. Fuso[b,*]

[a] *Department of Engineering and Architecture, University of Parma, Via delle Scienze 181/a, 43124 Parma, Italy*
[b] *Dipartimento di Fisica Enrico Fermi, Università di Pisa, Largo Bruno Pontecorvo 3, 56127 Pisa, Italy*

Abstract

An original model has been developed for the initial stage of bacterial adhesion on textured surfaces. Based on molecular dynamics, the model describes contact between individual bacterial cells in a planktonic state and a surface, accounting for both the mechanical properties of the cells and the physico-chemical mechanisms governing interaction with the substrate. Feasibility of the model is assessed via comparison with experimental results of bacterial growth on stainless steel substrates textured with ultrashort laser pulses. Simulations are performed for two different bacterial species, *Staphylococcus aureus* and *Escherichia coli*, on two distinct surface types characterised by elongated ripples and isolated nanopillars, respectively. Calculated results are in agreement with experiment outcomes and highlight the role of mechanical stresses within the cell wall due to deformation upon interaction with the substrate, creating unfavourable conditions for bacteria during the initial phases of adhesion. Furthermore, the flexibility of the model provides insight into the intricate interplay between topography and the physico-chemical properties of the substrate, pointing to a unified picture of the mechanisms underlying bacterial affinity to a textured surface.

Keywords: Antibacterial Surfaces, Molecular Dynamics, Textured Surfaces,

*Corresponding author:
Email address: francesco.fuso@unipi.it (F. Fuso)

1. Introduction

The requirement to contrast bacterial biofilm formation on surfaces is of vital importance in numerous fields including food processing machinery [1] and biomedical equipment, in particular in relation to post-surgical prosthetic infections [2]. The traditional approach to contrasting bacterial proliferation consists of charging the substrate with antimicrobials [3, 4, 5], a technique that suffers from limited duration, together with other side effects associated with antibiotic substances. The release of surface ions constitutes a valid alternative [6, 7, 8, 9, 10]; however, it is not without long-term side effects. A growing volume of literature is instead devoted to investigating the ability of micro and nanoscale textured surfaces to contrast biofilm formation [11, 12, 13, 14, 15, 16]. The concept behind this approach is that antibacterial behaviour depends on the size of surface protrusions. In particular, surface features whose sizes are smaller than that of individual bacterial cells inhibit bacterial attachment due to a reduction in the bacterium-substrate contact area based on simple geometric considerations, depicted schematically in Fig. 1(a). On the other hand, protrusions larger than the bacterial size may offer a larger contact area, as shown schematically in Fig. 1(b), and at the same time shelter against hydrodynamic shear flow, eventually promoting adhesion of cells in a planktonic state [11, 12]. Despite encouraging results obtained to date with this approach, correlation between bacterial adhesion and physico-chemical surface properties has not yet enabled adequate levels of predictability in the behaviour of processed surfaces. While several works have found clear correlations between roughness and retention of specific bacteria types [13, 14, 15, 16], others have found that surface roughness has negligible effects on adhesion [17, 18, 19].

A possible reason for such discrepancies may be found in the subtle interplay between surface topography and chemistry in determining the macroscopic behaviour of cell-substrate interactions. Changes in these properties are often

difficult to control individually and depending on the technique employed to generate the textured surface. Several studies have attempted to overcome this limitation by studying bacterial adhesion on perfectly regular textures [20, 21, 22, 23]; however, complete disentanglement of the two contributions is difficult to achieve within an experimental context.

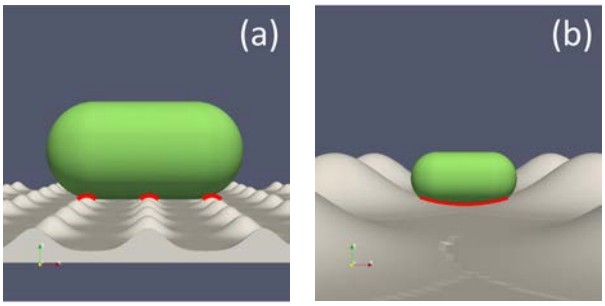

Figure 1: **Schematic representation of the contact area between a bacterial cell and textured substrate.** A single bacterial cell in contact with a rough substrate characterised by protrusions smaller (a) and larger (b) than the cell size. The cell-substrate contact area is highlighted in red.

Further to the above-mentioned complications, textured antibacterial surfaces are typically designed on the basis of a "zero-th order" bacterial model, where the cell is represented by an infinitely rigid body interacting with the substrate through simple geometric constraints. Recent experimental studies on naturally occurring antibacterial surfaces, such as cicada and dragonfly wings [24, 25, 26, 27], have revealed large deviations from the rigid body model owing to the presence of high aspect ratio protrusions with apical diameters in the order of a few tens of nanometres. Single bacterial cells in contact with textured surfaces experience mechanical stresses that are responsible for large deformations in their cell walls, leading to cell rupture in the most dramatic cases. However, it has been hypothesised [28] that even protrusions with smaller aspect ratios can result in stresses responsible for increased cell vulnerability or alterations in cellular metabolism. This hypothesis provides a wider interpretation of experimental results, including the inhibition of fimbrial production

induced by nanoscale topography [29] and the antibacterial properties of surfaces that are not themselves bactericidal. Furthermore, attractive forces in the order of hundreds of pN have been detected between single bacterial cells and substrates using Atomic Force Microscopy (AFM) [30, 31], which is much larger than the magnitude that would be expected in purely contact-type cell-surface interactions [32, 33].

In the case of individual colloidal particles interacting with perfectly flat substrates, the effects of surface chemistry have traditionally been described by the Derjaguin-Landau-Verwey-Overbeek (DLVO) theory, accounting for interplay between Lifshitz-Van der Waals and electrostatic forces. The more recent Extended DLVO (XDLVO) theory also accounts for Acid-Base (AB) interactions, which are considered the dominant contribution to attractive interactions [34, 35]. The Derjaguin approximation typically employed for XDLVO representations of extended objects, however, does not allow the description of interactions with rough substrates. Surface Element Integration (SEI) has been introduced to calculate the interaction energy between colloidal particles and textured surfaces [36, 37]. Within this approach, the antibacterial behaviour of textured surfaces is accounted for in terms of a reduction in the interaction energy for increasing values of average roughness [37]. The role of surface protrusion density in decreasing the cell-substrate contact area has also been predicted [37]. Other models have been developed to account for cell deformation in attempts to interpret bactericidal behaviour for nonrigid bodies [38, 39, 40], describing contact between a cell wall and patterned surface in terms of the minimisation of surface free energy. All of these models, however, are based on adaptation of the cell wall to well-defined textures, typically inspired by bactericidal biological surfaces [25] and modelled as regular arrays of simple geometric shapes. As a result, these approaches are inadequate when considering more irregular textures such as those produced via large scale processing in industrial contexts. Moreover, local non-covalent interactions with the substrate, considered in the DLVO-based approaches, are not taken into account, while fluid surrounding the cell, one of the most important mediators in the interaction

[41], is neglected.

To provide a more robust theoretical framework accounting for the antibacterial properties of industrially-relevant textured surfaces, this paper presents a model of bacteria-substrate interactions where bacterial cells are described as deformable objects in the framework of Molecular Dynamics (MD), overcoming limitations associated with the aforementioned approaches in view of a unified theory for the antibacterial properties of textured surfaces. Bacterial cells immersed in a computational fluid representing the surrounding environment interact with a computational substrate via specifically tailored physico-chemical processes. Owing to the spatial resolution enabled by the MD framework, the model allows the interaction energy of bacterial cells and surfaces to be determined in a manner that closely resembles experiments, without the need for geometric approximations. The feasibility of the approach is assessed by simulating the interaction of bacterial cells with surfaces chosen to represent stainless steel substrates textured with ultrashort laser pulses, shown to exhibit antibacterial properties in a previous work [16]. A statistical analysis is carried out considering a wide range of surface morphologies and different shaped cells. The mechanical properties of the latter were assigned based on currently available experimental data, with the antibacterial properties of each surface quantified in terms of local stresses acting on the bacterial cell walls. Dependence of simulation outcomes on parameters relating to surface chemistry leads to a novel interpretation of the antibacterial effects of textured surfaces.

2. Methods

Within the model, the cell was immersed in a computational fluid whose evolution in time was determined with the Lattice Boltzmann (LB) algorithm (version D3Q19) using the ESPResSo software [42].

The computational cell and cell-fluid coupling were introduced using the ESPResSo "object-in-fluid" package [43]. The simulation box was a parallelepiped of size $L_x = 2.5$ μm, $L_y = 3.8$ μm, and $L_z = 5.5$ μm. The physi-

cal properties of the computational fluid are summarised in the Supplementary Material. The cell was represented by a surface mesh with a node density of 204 μm^{-2}, sufficiently large to ensure adequate resolution of cellular deformation. The average area of a single mesh face was therefore $\sim 2.5 \times 10^{-3}$ μm^2, similar to the typical apical area of AFM tips employed to investigate the mechanical properties of single bacterial cells. As a consequence, direct comparison could be made between the stresses acting on single points of the cellular mesh and experimental data from external loads applied to single bacterial cells via AFM.

Each cell node interacted with adjacent nodes through forces given by the sum of various contributions, as discussed in detail in the Supplementary Material. Dominant contributions included the so-called stretching terms that depended on the distance between linked nodes, weighted with a proportionality factor k_s, and the bending terms that depended on the angle between mesh faces at a common edge, weighted with a factor k_b.

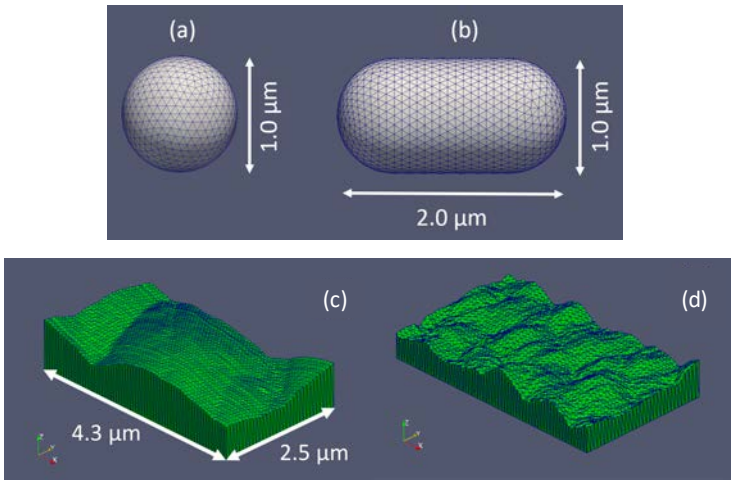

Figure 2: **Computational cells and substrates.** Images of meshes representing spherical (a) and spherocylindrical (b) model bacterial cells, and examples of substrates obtained by replicating portions of ShFM topographical maps [16]: LIPSS (c) and Nano-Pillars (NP) (d).

Simulations were performed for two distinct cellular geometries, represented graphically in Fig. 2: a spherical cell with a diameter of 1.0 μm [panel (a)] and

a spherocylindrical cell with a base diameter of 1.0 μm and a total length of 2.0 μm [panel (b)]. These two geometries and their relevant dimensions were chosen in line with experimental investigations [16], where the antibacterial behaviour of surface nanostructures was tested for spherical Gram-positive *Staphylococcus aureus* and spherocylindrical Gram-negative *Escherichia coli* bacteria.

The computational substrate was represented by a parallelepiped mesh of size 4.3 μm $\times$ 2.5 μm $\times$ 0.3 μm, comprising triangular faces with nodes acting as force centres for interactions with the computational cell. The substrate node density was the same as the cell node density, which was considered a compromise between the attainment of adequate surface resolution and the absence of computational artefacts (e.g. due to intersections between the cell and substrate meshes). An original Python code was developed to replicate measured topographical data on the upper face of the parallelepiped substrate so as to study the interaction of bacterial cells with substrates employed for experiments. Specifically, data acquired by Shear Force Microscopy (ShFM) on AISI 316L stainless steel substrates textured with ultrashort laser pulses [16] was employed. ShFM is a variant of scanning probe microscopy able to reconstruct surface morphology with nanometre spatial resolution [44]. Topographical maps used in the analysis consisted of 1024$\times$1024 discrete pixels with a spacing of 39 nm.

Two main surface feature classes were considered, Laser Induced Periodic Surface Structures (LIPSS) and Nano-Pillars (NP), having been identified as producing antibacterial effects for specific bacterial cell types [16]. LIPSS are elongated ripple-like surface protrusions that typically develop upon irradiation of metals or semiconductors with linearly polarised ultrashort laser pulses at fluence levels near the single-pulse ablation threshold. Their spatial period is generally slightly greater than half the laser wavelength, corresponding to about $0.8 - 0.9$ μm for a laser wavelength of 1064 nm in the present study. The height of such protrusions leads to a typical average areal roughness of $S_a \sim$ 90 nm. NP are instead isolated dot-like structures obtained through ultrashort laser processing with partial super-positioning of multiple, tangentially polarised

ultrashort laser pulses. The spatial separation of the NP considered within this study ranged from 0.8 to 1.3 μm, with feature heights corresponding to an average areal roughness of $S_a \sim 60$ nm [16]. The replication of small portions of the topographical maps on computational substrates is reported in Fig. 2 [panels (c) and (d)].

Within the model, the cellular mesh interacted with the substrate through the pairwise Lennard-Jones-like (LJ-like) potential

$$V(r_{ij}) = \begin{cases} \frac{C_1}{r_{ij}^{12}} - \frac{C_2}{r_{ij}^{6}} & r_{ij} \leq r_c \\ 0 & \text{otherwise} , \end{cases} \tag{1}$$

where r_{ij} represents the distance between the i-th cellular node and the j-th substrate node and r_c is a characteristic cutoff distance. Equation 1 differs from the classical Lennard-Jones (6,12) potential due to the presence of two parameters, C_1 and C_2, representing independently weighted repulsive and attractive terms, respectively.

Cell-fluid coupling was accounted for via a viscous force $\vec{F_i}$, whose expression for the i-th node was

$$\vec{F_i} = \xi(\vec{u}_i - \vec{v}_i) , \tag{2}$$

where $\vec{v}_i$ is the velocity of the i-th node, $\vec{u}_i$ the fluid velocity field in proximity of the i-th node and ξ the coupling coefficient.

A crucial aspect of the simulation dealt with assigning physically coherent values to the computational parameters governing mechanical properties of the cell and its interaction with the fluid and substrate, with different approaches employed to ascertain each parameter. Determination of the stretching and bending parameters, k_s and k_b, was accomplished through a calibration procedure based on simulation of Single Cell Force Spectroscopy (SCFS) experiments [45, 46, 47, 48]. For parameters C_1 and C_2 in Eq. 1, values were determined with a theoretical model based on summing all pairwise LJ-like interactions between cell and substrate nodes, the latter represented as a flat and infinite

mesh. By adopting a continuous approximation, this led to an integral for the total interaction potential between the whole cell and substrate as a function of their mutual distance. In order to validate the results, the modelled force vs. distance behaviour was compared with experimental force-displacement curves obtained in SCFS measurements [32, 49]. The adhesion force [32], defined as the minimum force for cellular detachment from a surface, and the work of adhesion, defined as the corresponding work [49], were used for evaluation of C_1 and C_2. Additional requirements were imposed to ensure computational stability and prevent unphysical behaviour such as intersections between cellular and substrate meshes. Finally, optimised values of ξ were determined based on the method proposed by Cimrák, et al. [50] involving calibration with a model for Stokes damping of ellipsoidal bodies in a fluid at rest. For the sake of conciseness, the above-mentioned techniques and the corresponding values of optimised computational parameters are discussed in detail in the Supplementary Material.

2.1. Simulation routine

The simulation of single cell-substrate adhesion events required definition of cell-substrate mechanical contact. In the initial stage of bacterial adhesion, the driving forces mediating the approach of a cell to the surface cannot be described analytically, since they mainly stem from stochastic processes such as Brownian motion and the dynamics of flagellar appendages [51]. It is therefore not possible to describe mechanical contact based on physically coherent driving forces. To overcome this limit, an original definition of contact was introduced.

From experimental data available in the literature, it was possible to retrieve information about the geometry of single bacterial cells adhered to flat substrates. Focused Ion Beam (FIB) tomography combined with SEM microscopy has been employed to obtain cross-sectional images of single spherical bacteria such as *S. aureus* [52] anchored on substrates. Contact-mode AFM topographical images of an *E. coli* bacterial cell were also available [53], enabling extraction of transverse topography profiles for different cellular conditions.

In the case of a spherical bacterium, cellular geometry at mechanical equilibrium was defined by the difference Δh between the vertical coordinates of the highest and lowest points of the cell. In the case of a spherocylindrical bacterium, cellular geometry was instead described by the sectional eccentricity e, defined as the ratio between the vertical and horizontal diameters, d_1 and d_2, of the elliptical section estimated from AFM topographical profiles. Using data from the literature [52, 53], values of $\Delta h/h_0 \sim 0.9$ μm and $e \sim 0.7$ were obtained, where h_0 is the undeformed cell diameter.

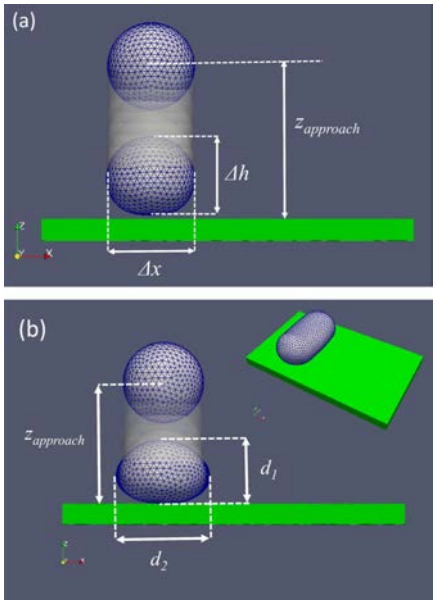

Figure 3: **Approach and contact on flat substrates.** Schematic representations of the preliminary phase of the simulation routine, necessary to define cell-substrate mechanical contact and the corresponding control parameters for spherical (a) and spherocylindrical geometry (b).

The simulation routine was divided in two distinct phases. In the first, the cellular mesh approached a perfectly flat computational substrate by exploiting the force exerted by the computational fluid flux perpendicular to the substrate plane. At each simulation step, Δh and e were used to monitor the geometry

of the spherical and spherocylindrical cells, respectively. The simulation was stopped when these parameters reached the values stated above within a 1 % tolerance, as shown in Fig. 3. Upon conclusion of this preliminary phase, the following parameters were retrieved for use in the subsequent phase: the intensity of the applied force $f_{approach}$, the number of steps required for completing the approach $N_{approach}$, and the initial distance between the centre of mass of the cell and the flat substrate $z_{approach}$. It must be noted that the only restriction relating to the choice of $f_{approach}$ was that the trajectory of cell nodes was sufficiently resolved to reach the required values of Δh and e within the specified tolerance.

Once the approach phase was completed, the second consisted of repeating the same procedure for a textured substrate with the same value of $f_{approach}$ as derived in the preliminary simulation. The initial distance between the centre of mass of the cell and the mean plane of the simulated topographical map was set to $z_{approach}$ and the simulation stopped upon reaching the number of steps $N_{approach}$. By maintaining all other simulation parameters constant, this procedure ensured equal simulation conditions for flat and textured substrates. Variations in the mechanical response of the cellular mesh and/or in the interaction with the substrate could therefore be attributed to the presence of the surface textures only.

The shape and spacing of the surface features affect adhesion through geometry, determining the probability that a cell makes contact with a protrusion or valley on the substrate. In order to account for inherent variations due to the irregular nature of each substrate, the same adhesion simulation was repeated 200 times for each substrate type, considering small portions of each surface that were randomly extracted from the experimental ShFM topographical map, with the results analysed statistically. Additionally, a random rotation parallel to the substrate mean plane was imposed on the spherocylindrical cell for each experiment to take into account shape anisotropy.

The effects of contact on individual nodes of the computational bacterial cells were quantified in terms of the total force, defined as a total f-metric value,

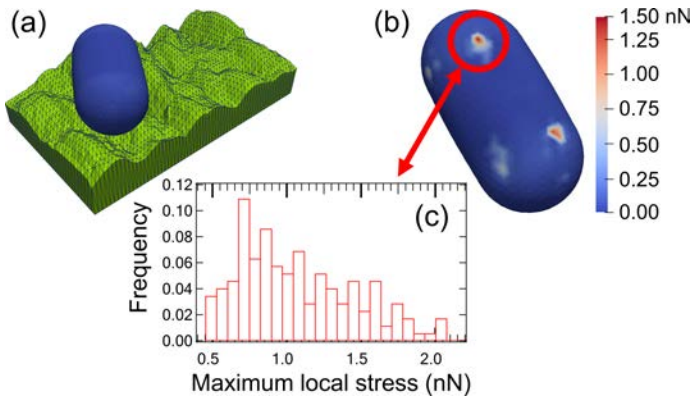

Figure 4: **Local stress on the cell wall.** Example of a spherocylindrical cell adhered to a substrate characterised by LIPSS (a), false colour map (b) representing the local stresses on the cell walls in an adhesion experiment and example of normalised frequency histogram of the maximum local stresses (c) produced with 200 simulations. The cell shown in (b) is rotated about its axis with respect to the cell shown in (a).

derived from stiffness interactions between cell nodes. The total f-metric was represented graphically as a false colour map superposed on the computational cell, an example of which is given in Fig. 4(a) and (b). Due to the local nature of stresses acting on the cell wall, the maximum value of the total f-metric, hereafter referred to as maximum local stress, was considered in the statistical analysis. As an example, Fig. 4(c) shows a frequency histogram of the maximum local stress on the cellular wall.

3. Results and Discussion

The routine discussed in Sec. 2.1 enabled simulations to be carried out where individual bacterial cells were made to adhere to different variants of textured substrates, calculating local stresses acting on the cell wall in each case. The investigation was based on the hypothesis that, with sufficiently high stress, unfavourable conditions for cellular adhesion would take place leading to enhanced antibacterial properties. As the computational substrates represented replications of specific experimental textures, a comparison could be made with

macroscopic investigations carried out in line with standard bacterial assays [16]. It must be noted, however, that the simulation focused on the initial stage of biofilm formation where bacterial cells were in a planktonic state and thus provided complementary information to experimental protocols, which were also affected by the subsequent bacterial colonisation stage.

3.1. Role of substrate roughness

For a given surface texture, the height of protrusions and therefore surface roughness is expected to affect cell adhesion. In order to ascertain the role of surface feature height on local stresses for an adhered cell, the topography of the experimental ShFM maps for LIPSS and NP was multiplied by a scaling factor M_z. $M_z = 1.0$ corresponded to the measured ShFM maps, while $M_z > 1.0$ corresponded to higher roughness and $M_z < 1.0$ to lower roughness.

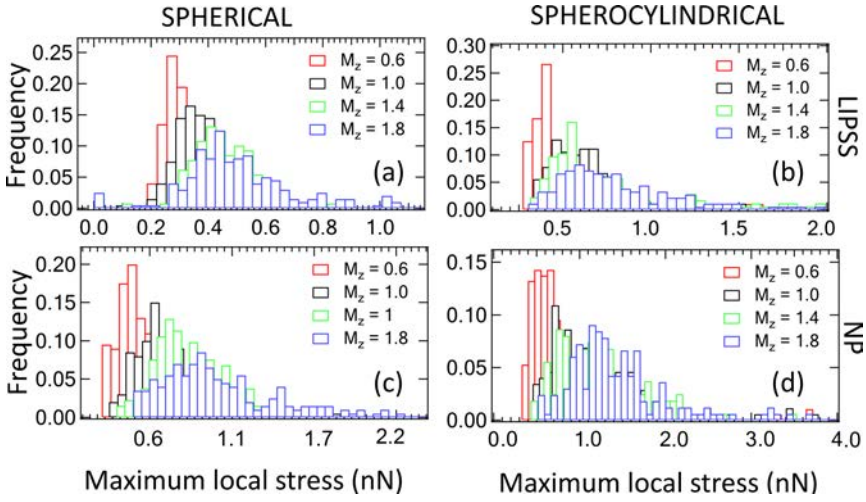

Figure 5: **Dispersion of data in 200 simulations.** Frequency histograms of the maximum local stress produced in 200 simulated experiments for the following combinations of cell geometry and surface texture: spherical - LIPSS (a), spherocylindrical - LIPSS (b), spherical - NP (c), spherocylindrical - NP (d).

For each of the 200 simulations performed in line with the procedure described in Sec. 2.1 for all combinations of substate, scaling factor and cell, the

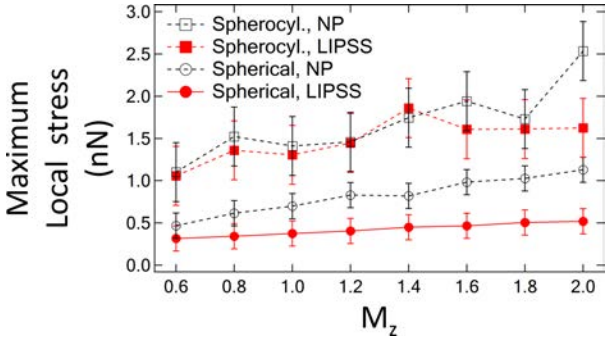

Figure 6: **Role of surface roughness.** Maximum local stress, averaged over 200 simulations, as a function of M_z for the four combinations of cell geometry and surface texture considered. Error bars correspond to the standard deviation over the statistical sample. Lines connecting data are intended as guides only.

maximum value of the local stress on each computational cell was extracted. Figure 5 presents histograms reporting the frequency for the maximum local stress observed in the simulations. Four values of M_z were considered for each combination of cell geometry and surface texture. It may firstly be noted that results are characterised by a large dispersion of values, reflecting fluctuations in morphology typical of laser-machined samples and the consequent randomness of the cell contact position. It is, however, evident that there is a shift in the distribution peak towards larger local stresses for increasing values of M_z and therefore surface roughness. This means that by vertically amplifying the topography, increasing the height of surface protrusions, a larger stress is induced in cell walls. This finding is confirmed by analysis of the maximum local stress as a function of M_z, averaged over the entire sample of 200 experiments, shown in Fig. 6. In addition to this outcome, the results highlight the presence of comparatively larger stresses for spherocylindrical geometry compared to spherical geometry at constant M_z.

Assuming that mechanical stresses play a dominant role in determining bacterial affinity to a textured surface, the above finding is in line with experimental outcomes presented within the literature [54], where spherical bacteria cells ex-

hibit higher mechanical strength compared to rod-like cells and possess higher adaptability to different textured substrates. Moreover, experimental results in [16], corresponding to $M_z = 1.0$ in the simulations, indicated a substantial difference between the antibacterial properties of substrates for *E. coli* and *S. aureus*, with the residual bacterial content systematically higher for spherical *S. aureus* than for the rod-like *E. coli* species. Simulation results show that the maximum local stress is around three times higher for spherocylindrical cells than for the spherical cells, which is in line with the original hypothesis that sufficiently high stress leads to unfavourable conditions for cellular adhesion.

In relation to the surface texture itself, results in [16] suggest a slightly more pronounced antibacterial effect for LIPSS than for NP, with residual bacterial counts slightly higher in the latter case for *E. coli*. Within the simulations, sensitivity to the surface texture was less evident for the spherocylindrical cell than for the spherical cell, with local stresses obtained for LIPSS and NP generally within their respective error bars independent of M_z. This outcome can be accounted for in terms of the larger degree of randomness within the simulation procedure for the spherocylindrical geometry, where the axis of the cell was randomly oriented over the substrate for each simulation, leading to a larger spread in the results. The longitudinal size of rod-like cells therefore leads to greater sensitivity to topographical fluctuations than for spherical cells within the finite sample of experiments considered. The simulations also suggest that NP are more "aggressive" than LIPSS for spherical cells, which is in general agreement with other experimental observations suggesting that an increase in the randomness of the texture, as is the case for NP, results in more pronounced antibacterial behaviour [55].

A key aspect to validating the hypothesis relating to the role of cell wall stress on antibacterial behaviour is linked to evaluation of the stress intensity so as to understand the extent to which values obtained in the simulation can be expected to cause changes in bacterial viability. Unfortunately, relevant data are not available in the literature as dedicated experiments are difficult to conceive. As mentioned above, however, the particular choice of mesh node

density enabled straightforward calibration of local stresses in physical units through simulation of SCFS experiments. A direct comparison between the local stress on a single mesh node and the external loads generally applied to individual bacterial cells in SCFS can therefore be carried out. Relevant literature suggests that bacterial cells are often subjected to external loads that do not exceed 2-3 nN [45, 46, 47, 48], with a few exceptions [56]. Since one of the requirements of SCFS is to maintain the cells alive during measurements, it can be assumed that such external loads do not to lead to cellular damage. Therefore, local stresses attained within the simulations are not expected to result in direct cytotoxic effects but are instead expected to lie within the range in which possible alterations in cellular metabolism can be induced, possibly responsible for the unfavourable environment leading to antibacterial behaviour [28].

3.2. Role of the physico-chemical surface properties

With the possibility of individually changing relevant parameters, the simulation represents a viable route to disentangling the effects of physico-chemical properties and surface morphology on bacterial adhesion. Surface chemistry is expected to play a role in cellular adhesion via different mechanisms. For instance, an increase in the repulsive nature of cell-substrate interactions might stem from variations in the ionic strength of the environment. Other possibilities include an increase in the volume of extracellular polymeric substances and therefore total steric repulsion range, or an increase in acid-base interactions associated with changes in surface wettability. The physico-chemical properties of the surface were determined within the model via the LJ-like potential in Eq. 1, where C_1 and C_2 were used to weight the repulsive and attractive terms, respectively, playing the role of control parameters. The results discussed in Sec. 3.1 were obtained with $C_1/C_2 = 2.4 \times 10^{-1}$ and $C_1/C_2 = 8.4 \times 10^{-4}$ (expressed in computational units with C_2 fixed to $3.1{\times}10^{-6}$) for the spherical and spherocylindrical cells, respectively. Such values were determined based on an optimisation procedure detailed in the Supplementary Material, leading to

a simulated adhesion force of $\lesssim$ 500 pN. Such a value, lying in the range of typical forces between a single *S. aureus* cell and human skin, is considered as corresponding to conditions of strong adhesion [32] and was therefore chosen as an upper limit. It must be emphasised that optimised values of C_1/C_2 depend on cellular geometry, despite referring to local node-node interactions, as they were determined based on macroscopic quantities including the cell-substrate adhesion force, which is representative of interaction between the whole cell and substrate.

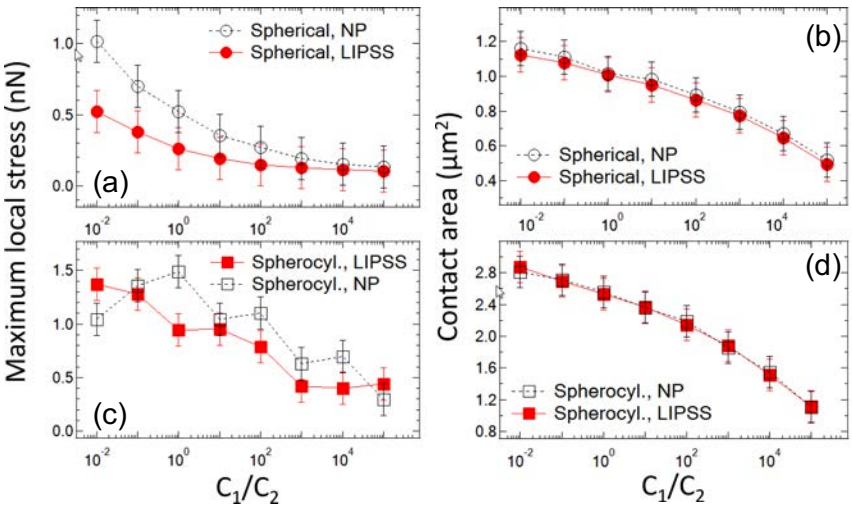

Figure 7: **Role of the repulsive/attractive interactions.** Maximum local stress and contact area, averaged over 200 simulations, as a function of the ratio C_1/C_2 (expressed in computational units with C_2 fixed to 3.1×10^{-6}) for spherical (a, b) and spherocylindrical (c, d) cells. Simulations were performed on computational substrates replicating LIPSS (red) and NP (black). Error bars correspond to the standard deviation over the statistical sample. Lines connecting data are intended as guides only.

Similar to the procedure outlined in Sec. 3.1, 200 simulations were carried out on textured surfaces with topographies replicated from ShFM maps ($M_z = 1.0$) for different values of C_1/C_2. According to the definition of mechanical contact in Sec. 2.1, the choice of C_1 and C_2 should in principle lead to different values of $N_{approach}$ at fixed $f_{approach}$ and $z_{approach}$. Therefore, for each tested value of

C_1/C_2, a specific procedure for determination of $N_{approach}$ was performed. Simulated surface interactions were varied by increasing C_1, starting from optimised values of C_1 and C_2. The range of variation in C_1/C_2, spanning several orders of magnitude, was tailored for each simulation condition in order to maintain numerical stability and prevent unphysical artefacts.

The maximum local stress, presented as an average of the 200 simulations in Fig. 7 for spherical and spherocylindrical cells [panels (a) and (c), respectively], decreases with increasing values of C_1/C_2 due to the increasingly repulsive nature of cell-substrate interactions. In the case of spherical geometry, the relationship between maximum local stress and C_1/C_2 is asymptotic for large values of the latter, which can be interpreted as representing the spatial region where the pairwise potential is non-zero. In fact, this envelope approaches a flat surface for large values of C_1/C_2, for which dependence of cellular behaviour on C_1/C_2 is lost for further increases in this ratio. Moreover, spherical cell geometry led to smaller dispersion of results, in agreement with the larger geometric adaptability of this cellular shape.

Further interesting interpretations can be drawn by studying the behaviour of the contact area between the cellular mesh and the substrate. In this work, the contact area was determined by employing the cutoff radius r_c for the pairwise LJ-like potential. The contact area was defined as the sum of the areas of the cellular mesh faces having all their three nodes located at a distance of less than r_c from at least one substrate node. Results are reported for the spherical and spherocylindrical geometries in Fig. 7 [panels (b) and (d), respectively]. In both cases, a small decrease in contact area was observed as the repulsive character of the interaction increased, even in the presence of large variations in the ratio C_1/C_2 and hence relevant modifications to the physico-chemical properties of the surface, with negligible dependence on the kind of surface features. It can also be noted that the contact area was systematically larger in absolute terms for the spherocylindrical geometry than for the spherical geometry. In comparison with the experimental results in [16], where the antibacterial behaviour of textured surfaces was found to be more evident for rod-like *E. coli*

than spherical *S. aureus*, the simulation results indicate that the absolute value of the contact area is not a meaningful parameter for predicting antibacterial properties.

A relevant conclusion that can be derived from the performed analysis is that a reduction in contact area with increasingly repulsive interactions corresponds to a reduction in the maximum local stress. Alternatively, this problem can be analysed in terms of the attractive component of the interaction energy, defined as the sum of the attractive contributions in the LJ-like potential, reported in the Supplementary Materials: the absolute value of this quantity decreases with increasing C_1/C_2.

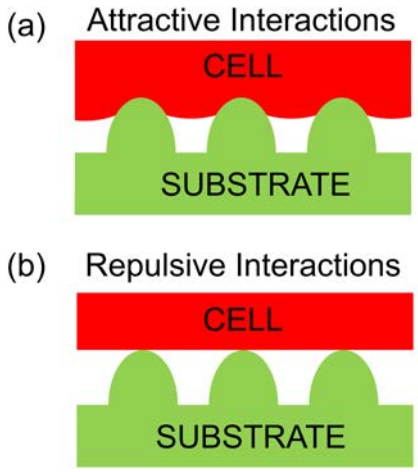

Figure 8: **Interplay between contact area and local stress.** Schematic representation of the two possible mechanisms responsible for antibacterial behaviour.

The whole set of results suggests a possible unified interpretation of the role of physico-chemical properties and surface roughness on the antibacterial properties of textured substrates. The schematic presented in Fig. 8 is intended to clarify the concept: when the chemical composition of the substrate determines local overall attractive interactions, the cell tends to be locally attracted towards the substrate, thus increasing mechanical stresses and eventually leading to un-

favourable conditions for cellular life. When the overall chemistry determines local repulsive interactions, the cell is locally repelled from the substrate and the mechanical configuration approaches a condition of interaction based exclusively on geometric contact. In this configuration, antibacterial behaviour can be interpreted according to the traditional approach based on reduced contact area facilitating cellular removal via hydrodynamic turbulence. Thus, antibacterial behaviour could result from interplay between the two effects: a stress-effect [Fig. 8(a)] and a geometric effect [Fig. 8(b)].

Bacterial cells are known to be able to modify their hydrophobicity within a certain range in order to adapt their surface chemistry to a substrate [57]. The model predicts that, within a certain range of cellular chemical compositions, a substrate can exhibit antibacterial behaviour through different mechanisms. Therefore, in the presence of sub-micrometric features, surface chemistry should play a minor role in determining overall antibacterial behaviour. This finding is in agreement with experimental results in [16], where two surfaces with the same geometry (LIPSS) but substantially different physico-chemical properties were tested. The first was hydrophobic, obtained by keeping the laser treated stainless steel substrates in air at room temperature for 30 days. The second was hydrophilic, obtained by keeping the laser treated substrates in water at 90 °C for 48 hours, a procedure able to promote the formation of hydrophilic iron oxides [58]. Both surfaces achieved low bacterial retention for rod-like *E. coli* but with negligible differences in antibacterial behaviour between the two. This outcome validates the hypothesis that chemistry plays a negligible role when textured substrates are considered.

4. Conclusions

Through implementation of MD tools, a unified model has been developed to simulate the initial stage of bacterial adhesion on textured surfaces. The model accounts for an extensive set of mechanisms at play on the nanoscale, including cell deformation, modelled in agreement with known mechanical properties of

selected bacteria, interaction with the fluid, playing an essential role in mediating the relevant dynamics, and interaction with the substrate, described through a potential with independently weighted attractive and repulsive contributions. The model represents a substantial step forward compared to conventional descriptions of cellular adhesion, which either consider bacteria to be rigid bodies and antibacterial behaviour to be the result of decreased contact area or consider bacterial to be deformable in the presence of regularly shaped textures. The occurrence of localised stresses on cellular walls, known to lead to unfavourable conditions for bacterial proliferation, can be reliably described as a function of topographical properties. The flexibility of the model, inherent in its ability to account for real surface textures, offers a viable approach for predicting the antibacterial properties of a wide range of substrates produced with practical processes. Individual adhesion experiments can be repeated over a statistical sample, accounting for morphological fluctuations typical of most large scale, high throughput processing technologies. Model validity was assessed based on stainless steel substrates textured with ultrashort laser pulses in a previous work [16], where pronounced antibacterial behaviour was reported, in particular for rod-like *E. coli* bacteria. The model demonstrates how the elongated shape of the bacteria leads to higher local stresses than for spherical cells, with implications for bacterial viability during the initial stage of adhesion.

The ability to individually manipulate a wide range of physical parameters via the MD approach paves the way to a robust, unified theory of the entire adhesion process. Simulation of the contact area and attractive interaction energy can be performed while tuning the interaction potential over a wide range of values to mimic variations in the physico-chemical properties of the surface. Simulation outcomes suggest that the antibacterial properties of textured substrates stem from interplay between strong local stresses for textured surfaces with mostly attractive potentials and reduced contact area for textured surfaces with mostly repulsive potentials.

Further work will be devoted to confirming model outcomes over a wider range of conditions, including substrates with higher roughness and spacing

such as those produced with longer laser pulses [59], as well as accounting for possible hydrodynamic effects eventually leading to detachment of initially adhered bacterial cells.

Acknowledgements

This research benefited from the HPC (High Performance Computing) facility at the University of Parma, Italy. This research did not receive any specific grant from funding agencies in the public, commercial, or not-for-profit sectors.

CRediT Author Statement

G. L.: Conceptualization; Methodology; Software; Formal analysis; Writing; Visualization. **A.H.A. L.**: Conceptualization; Methodology; Writing. **L. R.**: Conceptualization; Methodology; Writing; Supervision. **F. F.**: Conceptualization; Methodology; Writing; Supervision.

References

[1] Faille, C., Cunault, C., Dubois, T., & Bénézech, T. (2018). Hygienic design of food processing lines to mitigate the risk of bacterial food contamination with respect to environmental concerns. *Innovative Food Science & Emerging Technologies*, 46, 65-73. doi: 10.1016/j.ifset.2017.10.002.

[2] Arciola, C. R., Campoccia, D., & Montanaro, L. (2018). Implant infections: adhesion, biofilm formation and immune evasion. *Nature Reviews Microbiology*, 16(7), 397. doi: 10.1038/s41579-018-0019-y.

[3] Wang, B., Jin, T., Xu, Q., Liu, H., Ye, Z., & Chen, H. (2016). Direct loading and tunable release of antibiotics from polyelectrolyte multilayers to reduce bacterial adhesion and biofilm formation. *Bioconjugate Chemistry*, 27(5), 1305-1313. doi: 10.1021/acs.bioconjchem.6b00118.

[4] Vargas-Alfredo, N., Martínez-Campos, E., Santos-Coquillat, A., Dorronsoro, A., Cortajarena, A. L., Del Campo, A., & Rodríguez-Hernández, J. (2018). Fabrication of biocompatible and efficient antimicrobial porous polymer surfaces by the Breath Figures approach. *Journal of colloid and interface science*, 513, 820-830. doi: https://doi.org/10.1016/j.jcis.2017.11.050.

[5] Wang, B., Liu, H., Zhang, B., Han, Y., Shen, C., Lin, Q., & Chen, H. (2016). Development of antibacterial and high light transmittance bulk materials: Incorporation and sustained release of hydrophobic or hydrophilic antibiotics. *Colloids and Surfaces B: Biointerfaces*, 141, 483-490. doi: https://doi.org/10.1016/j.colsurfb.2016.02.021.

[6] Ferraris, M., Perero, S., Ferraris, S., Miola, M., Vernè, E., Skoglund, S., I. Odnevall & Wallinder, I. O. (2017). Antibacterial silver nanocluster/silica composite coatings on stainless steel. *Applied Surface Science*, 396, 1546-1555. doi: 10.1016/j.apsusc.2016.11.207.

[7] Xie, Y., Chen, L., Zhang, X., Chen, S., Zhang, M., Zhao, W., Sun, S. & Zhao, C. (2018). Integrating zwitterionic polymer and Ag nanoparticles on polymeric membrane surface to prepare antifouling and bactericidal surface via Schiff-based layer-by-layer assembly. *Journal of colloid and interface science*, 510, 308-317. doi: https://doi.org/10.1016/j.jcis.2017.09.071.

[8] Hikku, G. S., Jeyasubramanian, K., Jacobjose, J., Thiruramanathan, P., Veluswamy, P., & Ikeda, H. (2018). Alkyd resin based hydrophilic self-cleaning surface with self-refreshing behaviour as single step durable coating. *Journal of colloid and interface science*, 531, 628-641. doi: https://doi.org/10.1016/j.jcis.2018.07.089.

[9] Luo, Q., Cao, H., Wang, L., Ma, X., & Liu, X. (2020). ZnO@ZnS nanorod-array coated titanium: Good to fibroblasts but bad to bacteria. *Journal of colloid and interface science*, 579, 50-60. doi: https://doi.org/10.1016/j.jcis.2020.06.055.

[10] Khan, M. I., Mazumdar, A., Pathak, S., Paul, P., Behera, S. K., Tamhankar, A. J., Tripathy, S., Lundborg, C. S., & Mishra, A. (2020). Biogenic Ag/CaO nanocomposites kill Staphylococcus aureus with reduced toxicity towards mammalian cells. *Colloids and Surfaces B: Biointerfaces*, 189, 110846. https://doi.org/10.1016/j.colsurfb.2020.110846.

[11] Truong, V. K., Webb, H. K., Fadeeva, E., Chichkov, B. N., Wu, A. H. F., Lamb, R., Crawford, R, J., & Ivanova, E. P. (2012). Air-directed attachment of coccoid bacteria to the surface of superhydrophobic lotus-like titanium. *Biofouling*, 28(6), 539-550. doi: 10.1080/08927014.2012.694426.

[12] Lorenzetti, M., Dogsša, I., Stosšicki, T., Stopar, D., Kalin, M., Kobe, S., & Novak, S. (2015). The influence of surface modification on bacterial adhesion to titanium-based substrates. *ACS Applied Materials & Interfaces*, 7(3), 1644-1651. doi: 10.1021/am507148n.

[13] Liu, L., Ercan, B., Sun, L., Ziemer, K. S., & Webster, T. J. (2016). Understanding the role of polymer surface nanoscale topography on inhibiting bacteria adhesion and growth. *ACS Biomaterials Science & Engineering*, 2(1), 122-130. doi: 10.1021/acsbiomaterials.5b00431.

[14] Nguyen, D. H., Pham, V. T., Truong, V. K., Sbarski, I., Wang, J., Balčytis, A., Juodkazis, S., Mainwaring, D. E., Crawford, R. J., & Ivanova, E. P. (2018). Role of topological scale in the differential fouling of Pseudomonas aeruginosa and *Staphylococcus aureus* bacterial cells on wrinkled gold-coated polystyrene surfaces. *Nanoscale*, 10(11), 5089-5096. doi: 10.1039/c7nr08178b.

[15] Cuello, E. A., Mulko, L. E., Barbero, C. A., Acevedo, D. F., & Yslas, E. I. (2020). Development of micropatterning polyimide films for enhanced antifouling and antibacterial properties. *Colloids and Surfaces B: Biointerfaces*, 188, 110801. doi: https://doi.org/10.1016/j.colsurfb.2020.110801.

[16] Lutey, A. H., Gemini, L., Romoli, L., Lazzini, G., Fuso, F., Faucon, M., &

Kling, R. (2018). Towards laser-textured antibacterial surfaces. *Scientific Reports*, 8(1), 1-10. doi: 10.1038/s41598-018-28454-2.

[17] Flint, S. H., Brooks, J. D., & Bremer, P. J. (2000). Properties of the stainless steel substrate, influencing the adhesion of thermo-resistant streptococci. *Journal of Food Engineering*, 43(4), 235-242. doi: 10.1016/S0260-8774(99)00157-0.

[18] Verran, J., & Boyd, R. D. (2001). The relationship between substratum surface roughness and microbiological and organic soiling: a review. *Biofouling*, 17(1), 59-71. doi: 10.1080/08927010109378465.

[19] Hilbert, L. R., Bagge-Ravn, D., Kold, J., & Gram, L. (2003). Influence of surface roughness of stainless steel on microbial adhesion and corrosion resistance. *International biodeterioration & biodegradation*, 52(3), 175-185. doi: 10.1016/S0964-8305(03)00104-5.

[20] Friedlander, R. S., Vlamakis, H., Kim, P., Khan, M., Kolter, R., & Aizenberg, J. (2013). Bacterial flagella explore microscale hummocks and hollows to increase adhesion. *Proceedings of the National Academy of Sciences*, 110(14), 5624-5629. doi: 10.1073/pnas.1219662110.

[21] Hsu, L. C., Fang, J., Borca-Tasciuc, D. A., Worobo, R. W., & Moraru, C. I. (2013). Effect of micro-and nanoscale topography on the adhesion of bacterial cells to solid surfaces. *Applied and Environmental Microbiology*, 79(8), 2703-2712. doi: 10.1128/AEM.03436-12.

[22] Jin, L., Guo, W., Xue, P., Gao, H., Zhao, M., Zheng, C., Zhang, Y., & Han, D. (2015). Quantitative assay for the colonization ability of heterogeneous bacteria on controlled nanopillar structures. *Nanotechnology*, 26(5), 055702. doi: 10.1088/0957-4484/26/5/055702.

[23] Lee, J., & Pascall, M. A. (2018). Effect of micro-pattern topography on the attachment and survival of foodborne microorganisms on food contact surfaces. *Journal of Food Safety*, 38(1), e12379. doi: 10.1111/jfs.12379.

[24] Elbourne, A., Crawford, R. J., & Ivanova, E. P. (2017). Nano-structured antimicrobial surfaces: From nature to synthetic analogues. *Journal of colloid and interface science*, 508, 603-616. doi: https://doi.org/10.1016/j.jcis.2017.07.021.

[25] Ivanova, E. P., Hasan, J., Webb, H. K., Truong, V. K., Watson, G. S., Watson, J. A., Baulin, V. A., Pogodin, S., Wang, J. Y., Tobin, M. J. & Löbbe, C. (2012). Natural bactericidal surfaces: mechanical rupture of *Pseudomonas aeruginosa* cells by cicada wings. *Small*, 8(16), 2489-2494. doi: 10.1002/smll.201200528.

[26] Bandara, C. D., Singh, S., Afara, I. O., Wolff, A., Tesfamichael, T., Ostrikov, K., & Oloyede, A. (2017). Bactericidal effects of natural nanotopography of dragonfly wing on *Escherichia coli*. *ACS applied materials & interfaces*, 9(8), 6746-6760. doi: 10.1021/acsami.6b13666.

[27] Green, D. W., Lee, K. K. H., Watson, J. A., Kim, H. Y., Yoon, K. S., Kim, E. J., Lee, J., Watson, G. S., & Jung, H. S. (2017). High quality bioreplication of intricate nanostructures from a fragile gecko skin surface with bactericidal properties. *Scientific Reports*, 7(1), 1-12. doi: 10.1038/srep41023.

[28] Liu, Y., Strauss, J., & Camesano, T. A. (2008). Adhesion forces between *Staphylococcus epidermidis* and surfaces bearing self-assembled monolayers in the presence of model proteins. *Biomaterials*, 29(33), 4374-4382. doi: 10.1016/j.biomaterials.2008.07.044.

[29] Rizzello, L., Sorce, B., Sabella, S., Vecchio, G., Galeone, A., Brunetti, V., Cingolani, R., & Pompa, P. P. (2011). Impact of nanoscale topography on genomics and proteomics of adherent bacteria. *Acs Nano*, 5(3), 1865-1876. doi: 10.1021/nn102692m.

[30] Dufrêne, Y. F. (2014). Atomic force microscopy in microbiology: new structural and functional insights into the microbial cell surface. *MBio*, 5(4), e01363-14. doi: 10.1128/mBio.01363-14.

[31] Zhang, W., Stack, A. G., & Chen, Y. (2011). Interaction force measurement between *E. coli* cells and nanoparticles immobilized surfaces by using AFM. *Colloids and Surfaces B: Biointerfaces*, 82(2), 316-324. doi: https://doi.org/10.1016/j.colsurfb.2010.09.003.

[32] Formosa-Dague, C., Feuillie, C., Beaussart, A., Derclaye, S., Kucharíková, S., Lasa, I., Van Dijck, P., & Dufrêne, Y. F. (2016). Sticky matrix: adhesion mechanism of the staphylococcal polysaccharide intercellular adhesin. *ACS Nano*, 10(3), 3443-3452. doi: 10.1021/acsnano.5b07515.

[33] Camesano, T. A. (2019). Probing bacterial adhesion using atomic force spectroscopy. *Life at the Nanoscale: Atomic Force Microscopy of Live Cells*, 285. doi: 10.4032/9789814267977.

[34] Van Oss, C. J. (2006). *Interfacial forces in aqueous media*. CRC press. doi: 10.1201/9781420015768.

[35] Farahat, M., Hirajima, T., Sasaki, K., & Doi, K. (2009). Adhesion of *Escherichia coli* onto quartz, hematite and corundum: Extended DLVO theory and flotation behavior. *Colloids and Surfaces B: Biointerfaces*, 74(1), 140-149. doi: https://doi.org/10.1016/j.colsurfb.2009.07.009.

[36] Bendersky, M., & Davis, J. M. (2011). DLVO interaction of colloidal particles with topographically and chemically heterogeneous surfaces. *Journal of Colloid and Interface Science*, 353(1), 87-97. doi: 10.1016/j.jcis.2010.09.058.

[37] Siegismund, D., Undisz, A., Germerodt, S., Schuster, S., & Rettenmayr, M. (2014). Quantification of the interaction between biomaterial surfaces and bacteria by 3-D modeling. *Acta Biomaterialia*, 10(1), 267-275. doi: 10.1016/j.actbio.2013.09.016.

[38] Pogodin, S., Hasan, J., Baulin, V. A., Webb, H. K., Truong, V. K., Nguyen, T. H. P., Boshkovikj, V., Fluke, C. J., Watson, G. S., Watson, J. A., & Crawford, R. J., Ivanova, E. P. (2013). Biophysical model of bacterial cell

interactions with nanopatterned cicada wing surfaces. *Biophysical Journal*, 104(4), 835-840. doi: 10.1016/j.bpj.2012.12.046.

[39] Xue, F., Liu, J., Guo, L., Zhang, L., & Li, Q. (2015). Theoretical study on the bactericidal nature of nanopatterned surfaces. *Journal of Theoretical Biology*, 385, 1-7. doi: 10.1016/j.jtbi.2015.08.011.

[40] Li, X., & Chen, T. (2016). Enhancement and suppression effects of a nanopatterned surface on bacterial adhesion. *Physical Review E*, 93(5), 052419. doi: 10.1103/PhysRevE.93.052419.

[41] Cheng, Y., Feng, G., & Moraru, C. I. (2019). Micro-and nanotopography sensitive bacterial attachment mechanisms: A review. *Frontiers in Microbiology*, 10. doi: 10.3389/fmicb.2019.00191.

[42] Weik, F., Weeber, R., Szuttor, K., Breitsprecher, K., de Graaf, J., Kuron, M., Landsgesel, J., Menke, H., Sean, D., & Holm, C. (2019). ESPResSo 4.0–an extensible software package for simulating soft matter systems. *The European Physical Journal Special Topics*, 227(14), 1789-1816. doi: 10.1140/epjst/e2019-800186-9.

[43] Cimrák, I., Gusenbauer, M., & Jančigová, I. (2014). An ESPResSo implementation of elastic objects immersed in a fluid. *Computer Physics Communications*, 185(3), 900-907. doi: 10.1016/j.cpc.2013.12.013.

[44] Tantussi, F., Vella, D., Allegrini, M., Fuso, F., Romoli, L., & Rashed, C. A. A. (2015). Shear-force microscopy investigation of roughness and shape of micro-fabricated holes. *Precision Engineering*, 41, 32-39. doi: 10.1016/j.precisioneng.2015.01.003.

[45] Bailey, R. G., Turner, R. D., Mullin, N., Clarke, N., Foster, S. J., & Hobbs, J. K. (2014). The interplay between cell wall mechanical properties and the cell cycle in *Staphylococcus aureus*. *Biophysical Journal*, 107(11), 2538-2545. doi: 10.1016/j.bpj.2014.10.036.

[46] Wheeler, R., Turner, R. D., Bailey, R. G., Salamaga, B., Mesnage, S., Mohamad, S. A., Hayhurst E. J., Horsburgh, M., & Foster, S. J. (2015). Bacterial cell enlargement requires control of cell wall stiffness mediated by peptidoglycan hydrolases. *MBio*, 6(4), e00660-15. doi: 10.1128/mBio.00660-15.

[47] Liu, S., Ng, A. K., Xu, R., Wei, J., Tan, C. M., Yang, Y., & Chen, Y. (2010). Antibacterial action of dispersed single-walled carbon nanotubes on *Escherichia coli* and *Bacillus subtilis* investigated by atomic force microscopy. *Nanoscale*, 2(12), 2744-2750. doi: 10.1039/c0nr00441c.

[48] Deng, Y., Sun, M., & Shaevitz, J. W. (2011). Direct measurement of cell wall stress stiffening and turgor pressure in live bacterial cells. *Physical Review Letters*, 107(15), 158101. doi: 10.1103/PhysRevLett.107.158101.

[49] Rodriguez-Emmenegger, C., Janel, S., de los Santos Pereira, A., Bruns, M., & Lafont, F. (2015). Quantifying bacterial adhesion on antifouling polymer brushes via single-cell force spectroscopy. *Polymer Chemistry*, 6(31), 5740-5751. doi: 10.1039/c5py00197h.

[50] Cimrák, I., Gusenbauer, M., & Schrefl, T. (2012). Modelling and simulation of processes in microfluidic devices for biomedical applications. *Computers & Mathematics with Applications*, 64(3), 278-288. doi: 10.1016/j.camwa.2012.01.062.

[51] Berne, C., Ellison, C. K., Ducret, A., & Brun, Y. V. (2018). Bacterial adhesion at the single-cell level. *Nature Reviews Microbiology*, 16(10), 616-627. doi: 10.1038/s41579-018-0057-5.

[52] Gu, J., Valdevit, A., Chou, T. M., & Libera, M. (2017). Substrate effects on cell-envelope deformation during early-stage *Staphylococcus aureus* biofilm formation. *Soft Matter*, 13(16), 2967-2976. doi: 10.1039/c6sm02815b.

[53] Van Der Hofstadt, M., Hüttener, M., Juárez, A., & Gomila, G. (2015). Nanoscale imaging of the growth and division of bacterial cells on planar

substrates with the atomic force microscope. *Ultramicroscopy*, 154, 29-36. doi: 10.1016/j.ultramic.2015.02.018.

[54] Fadeeva, E., Truong, V. K., Stiesch, M., Chichkov, B. N., Crawford, R. J., Wang, J., & Ivanova, E. P. (2011). Bacterial retention on superhydrophobic titanium surfaces fabricated by femtosecond laser ablation. *Langmuir*, 27(6), 3012-3019. doi: 10.1021/la104607g.

[55] Rajab, F. H., Liauw, C. M., Benson, P. S., Li, L., & Whitehead, K. A. (2018). Picosecond laser treatment production of hierarchical structured stainless steel to reduce bacterial fouling. *Food and bioproducts processing*, 109, 29-40. doi: 10.1016/j.fbp.2018.02.009.

[56] Coldren, F. M., Foteinopoulou, K., Verbeeten, W. M., Carroll, D. L., & Laso, M. (2008). Modeling the effect of cell-associated polymeric fluid layers on force spectroscopy measurements. Part II: experimental results and comparison with model predictions. *Langmuir*, 24(17), 9588-9597. doi: 10.1021/la800944q.

[57] Krasowska, A., & Sigler, K. (2014). How microorganisms use hydrophobicity and what does this mean for human needs?. *Frontiers in cellular and infection microbiology*, 4, 112. doi: 10.3389/fcimb.2014.00112.

[58] Kietzig, A.-M., Hatzikiriakos, S. G. & Englezos, P. (2009). Patterned superhydrophobic metallic surfaces. *Langmuir*, 25(8), 4821–4827. doi: 10.1021/la8037582.

[59] Romoli, L., Lazzini, G., Lutey, A. H. A. & Fuso, F. (2020). Influence of ns laser texturing of AISI316L surfaces for reducing bacterial adhesion. *CIRP Annals*, 69(1), 529-532. doi: 10.1016/j.cirp.2020.04.003.